DE GRUYTER

High Temp. Mater. Proc. 2017; 36(4): 399–409

Runnan Wang, Xuewei Yan, Zhonglin Li, Qingyan Xu* and Baicheng Liu

Effect of Construction Manner of Mould Cluster on Stray Grain Formation in Dummy Blade of DD6 Superalloy

Abstract: A dummy blade of Ni-based single crystal (SX) superalloy was modelled to investigate the stray grain (SG) defect by both experiment and simulation. Three construction manners of mould cluster (CMMC) with 0°, 45° and 90° assembling angle were considered. The experimental results reveal a strong dependence of SG sensitivity upon CMMC. Profuse SGs took place in the case of 0°, but almost no one shown in those of 45° and 90°. The FEM simulation results indicate that SG occurrence is not only determined by critical nucleation undercooling, but also the geometrical characteristic, shape of liquidus isotherm and other three important effects (shadow effect, channel effect and dimension effect). The tendency of SG formation increases with the increase of number of these effects. By means of the combination effect consisting of the above three effects, SG occurrence can be qualitatively predicted and process window is more accurately modified.

Keywords: single crystal, stray grains, numerical simulation, combination effects, process window

Introduction

Ni-based single crystal components are of great importance to gas turbine blade due to their excellent performance resistant to creep, rupture, corrosion and oxidation [1]. It consists of a face centred cubic (FCC) structured matrix phase (γ phase), and $L1_2$ super-lattice structured strengthened precipitated phase (cuboidal,

intermetallic γ' phase) appeared as coherency lattice with γ phase [2]. However, most process related defects such as stray grain (SG) [3, 4] freckles [5, 6] silver [7] and recrystallization [8] are prone to occur during directional solidification. SG is one of the most harmful defects, whose occurrence can introduce new high-angle boundaries and severely reduce the performance of SX component, due to the reduction of grain boundary strengthened elements in SX superalloy.

According to many previous researches, SG have been mostly investigated in seed crystal technology [9–11], weld manufacturing [12–14] and corresponding microstructure [15–19]. Meanwhile, in order to suppress SG formation, some methods are developed such as grain continuator [20] and heat conductor [21]. Using grain continuator can prevent the formation of SGs, but probably increase the tendency of forming low-angle grain boundaries (LABs) [20, 22, 23] at the same time, which are detrimental to the high-temperature mechanical properties of components [24, 25]. Most work to date focused on the research of simple and ideal system, but industrial conditions and casting are significantly more complex. In addition, few studies have attempted to relate mould cluster's assembly to the mechanisms of SG formation in platform systematically, nevertheless, how to control both grain structure and microstructure requires an accurate understanding of this relationship during solidification.

In this research, the effect of different CMMC on SG formation in a cross-section enlargement during directional solidification was further studied. The experiment with variable construction manners were performed, followed by numerical simulation for intuitively observing and data obtaining during invisible solidification process. By both experimental and simulation methods, three effects (shadow effect, channel effect and dimension effect) are proposed to account for the variation of SG occurrence among three forms of CMMCs. Predicting SG sensitivity will then be discussed through combined superposition effect considering the above three effects. Besides, process window is modified using both proposed model and experimental results.

*Corresponding author: Qingyan Xu, Key Laboratory for Advanced Materials Processing Technology, Ministry of Education, School of Materials Science and Engineering, Tsinghua University, Beijing 100084, China, E-mail: scjxqy@tsinghua.edu.cn
Runnan Wang, Xuewei Yan, Zhonglin Li, Baicheng Liu, Key Laboratory for Advanced Materials Processing Technology, Ministry of Education, School of Materials Science and Engineering, Tsinghua University, Beijing 100084, China

Experimental procedure and simulation method

The second generation Ni-based single crystal superalloy DD6 was employed, with nominal composition given in Table 1. In order to study the influence of placing direction of components (Figure 1) on the formation of SGs, a series of directional solidification experiment with DD6 was performed using an industrial vacuum Bridgman furnace, with various assembling angle in direction between component and mould cluster radial. Three forms of CMMC designated as Cluster A, Cluster B and Cluster C (representing that the components in each cluster were assembled misaligned of 0°, 45° and 90° (Figure 2), with regard to the radial direction, respectively) were directionally solidified. For each mould cluster, four specimens are constructed in it around a central rod by fourfold symmetry.

Table 1: Nominal composition of superalloy DD6 [27].

Element	Cr	Co	Mo	W	Ta	Re	Nb	Al	Hf	Ni
wt. %	4.3	9	2	8	7.5	2	0.5	5.6	0.1	Balance

The size detail of the wax model of the specimen geometry is presented in Figure 1, with a length of 99 mm, approximately equal to the length of turbine blade of aircraft engine. The wax models were fabricated b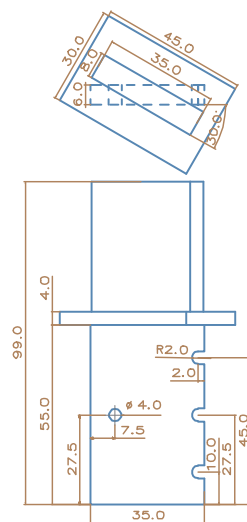y 3D printing additive manufacturing technology, and the ceramic shell was produced by a standard investment casting procedure. Some special geometrical structures were introduced into the model, such as grooves and holes (Figure 1), so as to model the complicated airfoil characteristics and stress concentration zone where defects tend to occur. The temperature of pouring, upper and lower heater was set at 1,550 °C, 1,530 °C and 1,550 °C, respectively. After preheating, pouring and heat preservation, chill, ceramic shell and alloy were withdrawn from heating zone to cooling zone through baffle at a constant velocity rate of 5 mm/min.

After the casting process, the specimens were chemical macro-etched using a solution of HCl (90 %) and H_2O_2 (10 %) to examine SG formation. Besides, a cuboid piece was cut off from some samples using Electrical Discharge Machining (EDM) to perform the EBSD for grain micro orientation measurement. The inner face of cut specimen was ground to a 2000# finish, followed by mechanical polishing and electro-polished using $HClO_4$ (10 %) and C_2H_5OH (90 %) [26] to attain a defect-free flat surface for grain orientation measurement. The specimen was examined by an Oxford detector within a Merlin scanning electron microscope. EBSD measurement was performed under 10~25 μm to obtain a good combination of accuracy and collection time.

Commercially available finite element method software (ProCAST) was used for the simulation of thermal field and fluid flow during directional solidification. The model and mesh employed are presented in Figure 3. Results extracted from the FEM calculation were transferred to CAFÉ (cellular automaton finite-element) post-module to predict grain morphology, as well as the evolution of grains competing growth. For the accuracy of calculating, measured temperature-dependent boundary conditions were employed. Besides that, the superalloy's thermophysical parameters were from books [27, 28].

Experimental results and simulations

Stray grain formation

SG formation in the platform of the model with different assembling angle is shown in Table 2. Stray grains particularly occur at the places of abrupt transition such as platforms, and SG sensitivities obviously vary with construction manners. Cluster A (0°) shows the strongest tendency for SGs among all three cases, because SGs
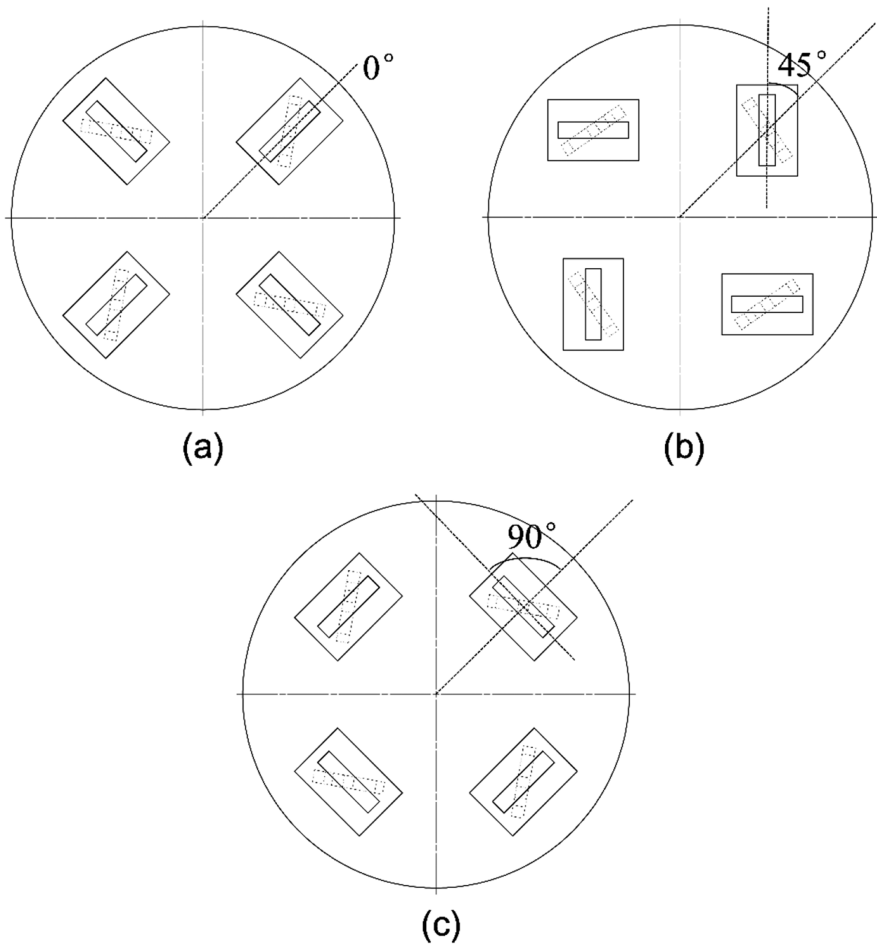

<center>(a)</center> <center>(b)</center>

Figure 1: (a) The wax model and (b) size detail of the sample.

Figure 2: The constructing manner of mould cluster (a) A, (b) B and (c) C, with the deviation (assembling) angle of 0°, 45° and 90°, respectively.
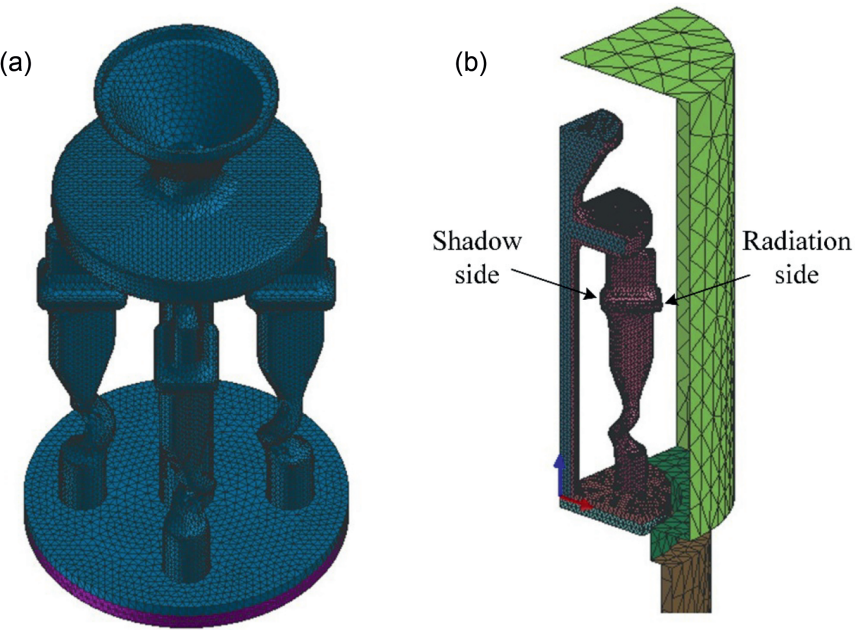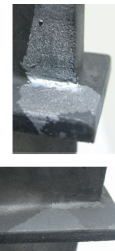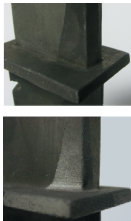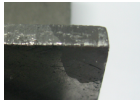

Figure 3: The mould cluster (a) A (0°), with four specimens named A1~A4, and (b) its calculation unit, a quarter of the fourfold symmetric model.

Table 2: Variation of SG formation with different CMMCs, where SD, SN and MI denote shadow side, radiation side (Figure 3(b)) and middle area, respectively. The CA simulation of solidified grain structure in DD6 superalloy is also tabulated.

Sample / Cluster	1	2	3	4	Simulation
A(0°)	SD, MI	SD	SD, SN	SN	
B(45°)	No SG	No SG	No SG	No SG	
C(90°)	SN	No SG	No SG	No SG	

were detected in all the four components. However, the other two cases (cluster B and C, with 45° and 90° deviation angle, respectively) display the opposite phenomenon, with no SGs forming in Cluster B, and appearing only one of four samples in Cluster C. This experimental results differed from the CA simulation results listed in the last column of Table 2. It is also found that most SGs are likely to nucleate at platform end (shadow side and radiation side), then grow into tenon. Generally, stray grain belonged to one nucleation occupy no more than a quarter of platform. The above phenomenon reveals that the formation of SGs in the platform of the same samples depends sensitively on CMMC even using identical process parameters. This also indicates that the solidification condition are unlike each other in different CMMCs, which may influence not only the SG sensitivity, but also the microstructure and mechanical property.

Micro-orientation within platform

A small cuboid specimen for EBSD was cut off from sample A3 (0°) and B1 (45°) using Electrical Discharge Machining (EDM) to investigate the orientation of primary and stray grain within the platform with early
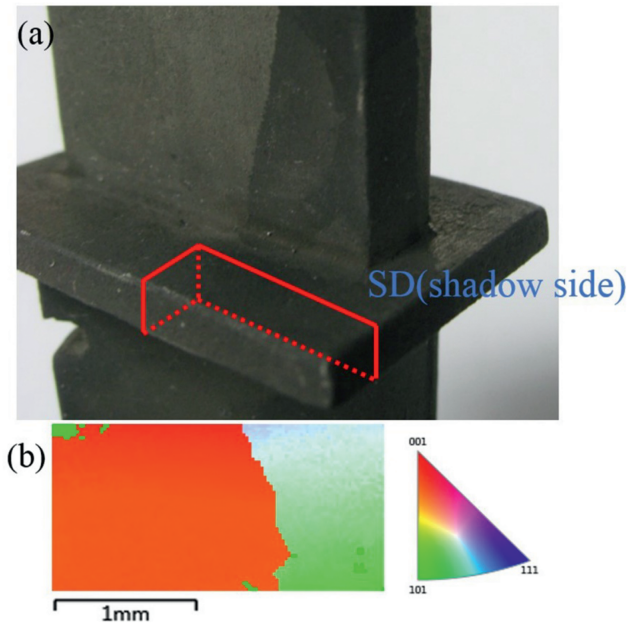
Figure 4: For sample A3, (a) the location of cut specimen for EBSD measurement and (b) corresponding orientation map of inner face of it.

Figure 5: Three Euler angles vary with the selected points in the cut specimen of sample B1.

supercooling. The orientation map is shown in Figure 4, the red area represents the primary grain which aligns well with (001), and SG is marked with green. The evolution and morphology of grain boundary between primary and stray grain is clearly characterized by colour contrast. Severe early supercooling in platform end, gives rise to rapid growth of new nucleation, and leads to LAB (low-angle boundary) in this region, shown as gradual variation of green colour within SG. Five specified points of platform end in sample B1 are selected to perform EBSD measurement, and three Euler angles were obtained as well (Figure 5). It reveals that three Euler angles all continuously change with the increase of the distance from one edge of specimen, particularly, there is an obvious decrease of Phi2 (~8 % from point 1 to point 5), indicating the existence of LAB in SG-free sample owing to large undercooling and rapid unstable dendritic growth in this area.

Shape of mushy zone in airfoil

For the airfoil, the isotherm contours of numerical results are presented in Figure 6, as well as the shape of mushy zone and solidification sequence, which will influence grain nucleation and growth. Compared with the sample B (45°), the liquidus isotherm of sample A (0°) and C (90°) appeared greater tilt angel of 13° and 9° in the
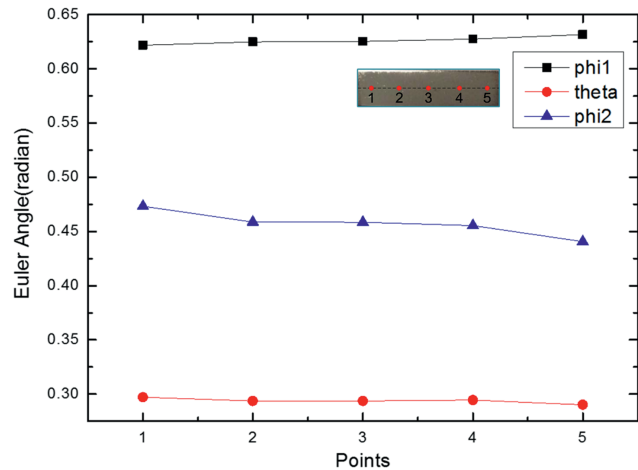
upper airfoil, respectively. It can be derived that at the time when primary grain approaches to platform, the volume of primary grain front is smaller. In particular, the part of mushy zone towards the cluster centre, appears as higher position due to the lack of heat radiation. Meanwhile, the opposite side of sample, as a result of abundant heat radiation, has higher temperature and lower position of mushy zone. In Figure 6(b), both sides of liquid/solid interface are little higher than middle of that, inducing a concave shape in airfoil.

Characteristic of solidification near platform

As shown in Figure 7, the temperature distribution and evolution of mushy zone around platform during cooling process is presented, as well as the location of selected specified points on the lower surface of platform end and the junction of platform and airfoil. Within platform and on the surface of that, four points, SDC (corner of shadow side), SDR (junction of shadow side), SNR (junction of radiation side) and SNC (corner of radiation side), were selected to investigate the transformation of liquid/solid interface morphology. Figure 7 also implied that, under three forms of CMMCs, the part of samples all exhibit early cooling in the area towards furnace centre, and hysteretic cooling in the region of opposite direction, owing to the line of SDC.

The simulated results showed that the external edge of model which faced towards the furnace was cooled faster in the heating zone and slower in the cooling zone, compared with the inner part of the cluster. The shape of mushy zone appears simple form in airfoil, but becomes
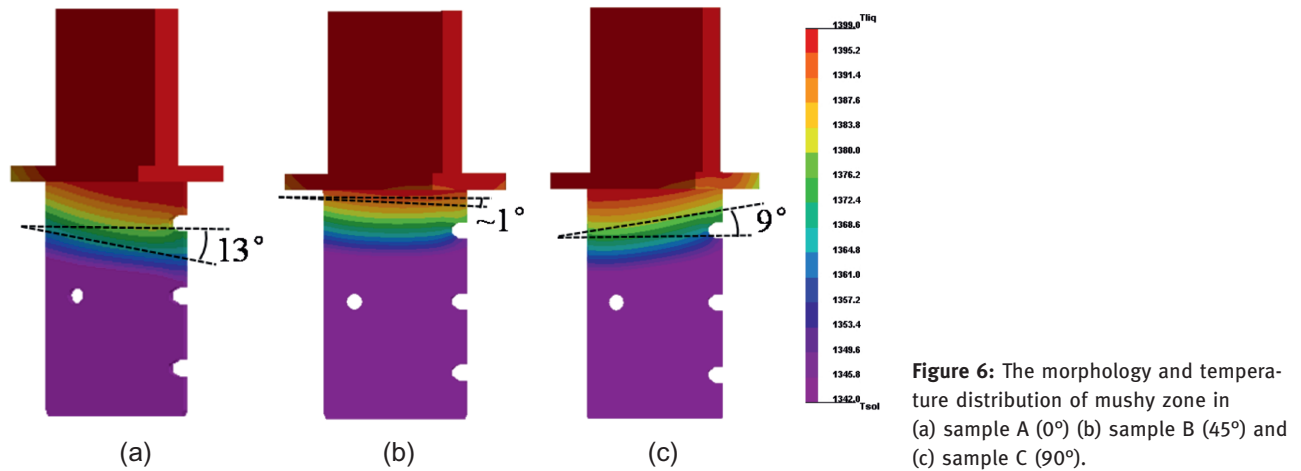
Figure 6: The morphology and temperature distribution of mushy zone in (a) sample A (0°) (b) sample B (45°) and (c) sample C (90°).
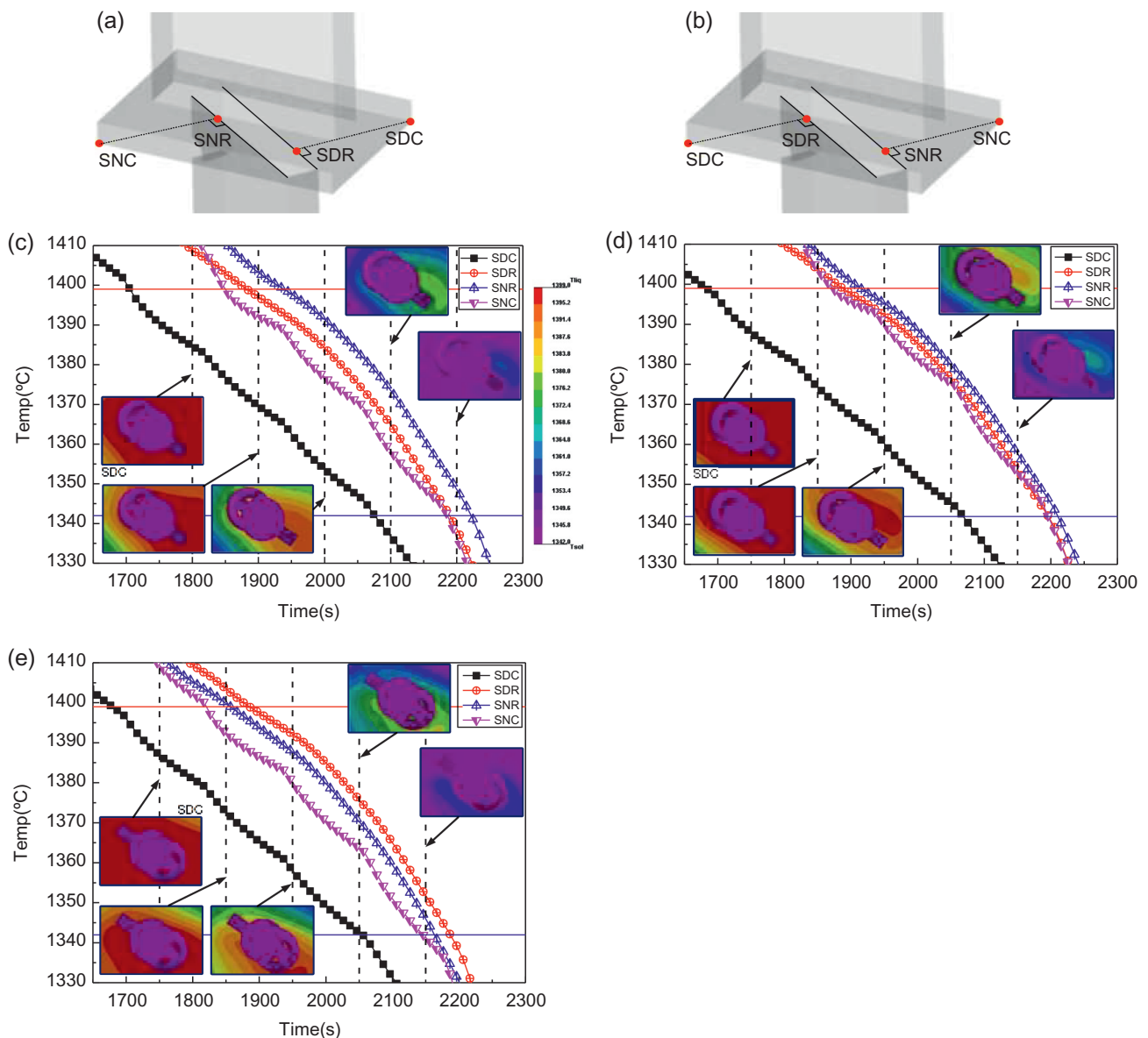

Figure 7: Temperature varies versus time in four specified points that located in the platform of sample (a) (c) A, (a) (d) B and (b) (e) C.
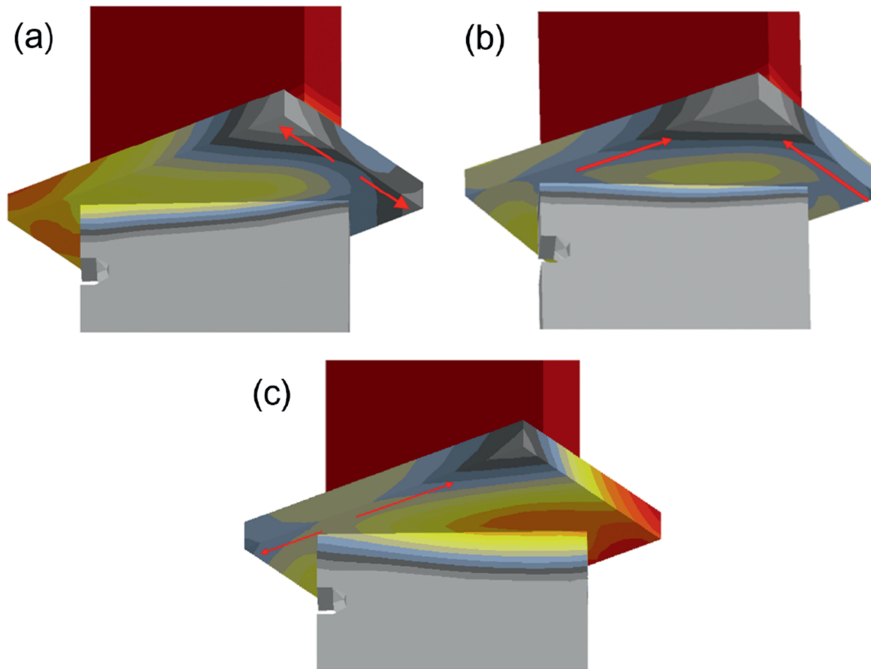
Figure 8: Cooling channels for primary grain growing which are mainly influenced by solidification sequence, corresponding to the sample of Cluster (a) A (0°), (b) B (45°) and (c) C (90°).

more complex when sectional enlargement occurs, as shown in Figure 8, that is, solidification condition varies intensively in particular area.

Discussion

The location and deviation angle of component in the cluster assembly significantly influence the cooling path and morphology of mushy zone during directional solidification. General nucleation model in terms of supercooling [29,30] can't perfectly account for the experimental phenomenon, so the following effects are proposed to help investigate the solidification process and the mechanism of grain growth.

Shadow effect

Most heat flux in heating zone comes from the radiation produced by heater, and shine the samples on surfaces. However, due to the N-fold symmetric construction manner of mould cluster, the central part of cluster becomes a shadow region, which keeps most radiation heat flux away. The non-uniform solidification condition will be induced, appearing as the difference of undercooling/temperature between shadow and radiation side in the same horizontal plane perpendicular to withdrawing direction. It means that serious early undercooling is more likely to occur at shadow side, and have detrimental effect on SG formation. Figure 7 shows that the temperature at the platform exposed to heater side is approx. 20 °C higher than that towards the shadow side, and the simulated results agreed well with the experimental results [4].

Besides the early undercooling at the sided corner or the edge of platform, the liquid/solid interface displays different morphology and position due to shadow effect. There are relatively bigger tilt angle (13° and 9°, respectively) of the mushy zone in sample A and C, compared with sample B. Big tilt angle of mushy zone will induce only a small volume of primary grain of solidification front that can grow into the platform at early stage, as shown in Figure 6(a) and (c). It represents a non-horizontal solidified interface, and breaks the uniform solidification condition at the junction area of airfoil and platform. On the contrary, the samples in Cluster B, whose airfoils have the shortest length in the radial direction of mould cluster among three CMMCs, present the liquidus isotherm most similar shape to flat (Figure 6(b)), which has beneficial effect on SG suppression. Therefore, it is deduced that the SG tendency increases and volume fraction of primary grain decreases with the increase of the tilt angle of mushy zone.

For sample A, B and C, the deviation angle (φ_d) between the airfoil and tangent direction of cluster are

calculated to be 60°, 15° and 30°, respectively. This angle, combined with size of platform, leads to variable cooling condition around the junction area and significantly influence the intensity of shadow effect. The tilt angle of liquidus isotherm in airfoil increases with the increase of φ_d.

Channel effect – First stage for dendritic branching

The reports related to the solidification and casting addressed the impact of local undercooling on SG formation in platform, and regarded it as the dominating criterion for the onset of SG nucleation [31,32], whilst other factors were rarely considered. As referred above, for the samples in Cluster A and C, SGs were detected in platform intuitively, nevertheless, no SG defect found was in Cluster B, despite big undercooling exits within the platforms for all three CMMCs. In order to account for this difference and SG formation sensitivity, channel effect is proposed and employed after shadow effect. As a connection between primary grain (airfoil) and undercooled region (corner of platform), the feeding (cooling) channels can provide paths for grain growth.

As seen in Table 2, the SGs mostly occur at the platform end where best heat dissipation condition appears, inducing the existence of local high undercooling until the mushy zone from airfoil approaches. Besides, based on the inclined shape of mushy zone and relevant solidification sequence in platform, the amount of primary grains that grows into the platform is reduced as a result of big tilt angle of mushy zone, thus, leading to bad feeding rate for sample A(0°) and C (90°). Furthermore, the solidification conditions, paths and sequences for three CMMCs are quite different, as shown in Figure 8. The platforms in sample A and C both exhibit single edge cooling (Figure 8(a) and (c)), and this form of solidification significantly decreases the number of cooling (feeding) channels connecting the undercooled area and primary grain. However, the samples in Cluster B (45°) whose platforms cool along both two edges (Figure 8(b)), can be highly efficiently fed by the solid front, together with the mushy zone of flat shape. This form of solidification, combined with relatively simultaneous uniform solidification condition around platform, will provide more feeding channels. As a result, although the shadow effect obviously leads to high undercooled corner isolated from primary mushy zone (Figure 7(b)) as well, none of the four samples in Cluster B exhibits SG.

Dimension effect – Second stage for dendritic branching

Furthermore, the platforms have both long and short edges, which will induce an effect on the solidification sequence. For the samples in Cluster C, the long edge of platform solidified prior to the short one, and experimental results display no SGs. In contrast to this, all the samples in Cluster A with almost the same tilt angle of mushy zone, exhibit profuse SGs under identical solidification conditions. The only difference between these two clusters is the CMMC. This leads to the short edge of platform solidified first in Cluster A, but the long edge solidified first in Cluster C, as shown in Figure 9(a) and (b). Then, the solidified parts will extend to the other side along the long and short edge, consume long and short time in Cluster A and C, respectively. Figure 9 clearly illustrates the path along which the mushy zone moves, indicating the impact of dimension on the solidification condition and sequence. The finding and analysis in this study agree well with Meng's conclusions [33]. By comparing the same samples employed different CMMCs and
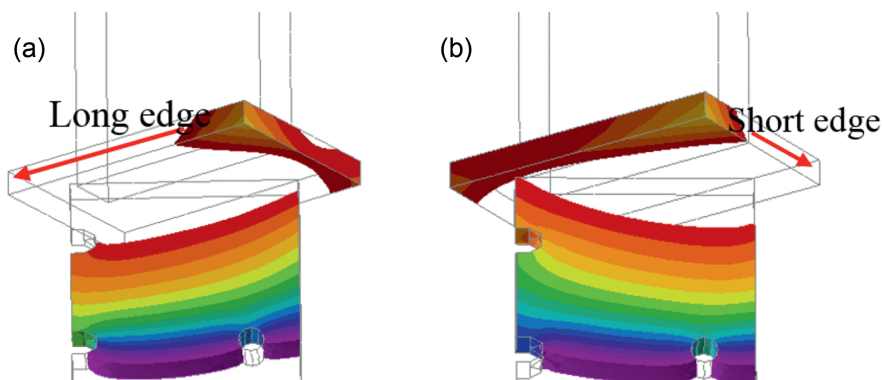

(a) Long edge

(b) Short edge

Figure 9: Solidification sequence around platform of sample (a) Cluster A (0°) and (b) Cluster C (90°), depicted by the contour of simulation results.

identical process parameters, it is deduced that deviation angle is obviously crucial to the quality and defect formation of the component.

Combination effect

Corresponding to the experimental results in this study, three effects are listed in Table 3 to examine the SG sensitivity, with regard to three forms of CMMC. As shown, three effects are all "Positive" in Cluster A, corresponding to the strongest SG tendency, revealing that all the effects are prone to SG formation. However, there are only one and two "Positive" in Cluster B and C, respectively, explaining the weaker tendency for SG occurring. Taken together this is evidence that three effects interact with each other instead of working alone during directional solidification, and result in alternative tendency of SG formation.

Table 3: SG sensitivity associated with combination effect for three forms of CMMCs, where P and N denote positive and negative, respectively.

Cluster	Shadow effect	Channel effect	Dimension effect	Formation of SG
A (0°)	P	P	P	Much
B (45°)	P	N	N	Null
C (90°)	P	P	N	Rare

Model illustrating and predicting the SG formation in platform of single crystal component is established, considering the shadow effect, channel effect and dimension effect in sequence. The CMMC, independent of other process parameters such as the pre-set temperature and withdraw rate, plays a dominant role during casing and leads to variable qualities of component. The proposed model, in which three effects are considered, may provide a powerful tool for SG prediction during directional solidification.

Process window and model for predicting SG

Based on the growth kinetics of the dendrite tips given by Kurz-Giovanola-Trivedi (KGT) model [34] and some assumptions, Bussac and Gandin [35] established a model for predicting the SG occurrence from the view of dendritic growth, with a mathematical expression given by:

$$l(\Delta T_{nucl}) = \int_{to}^{t_{nucl}} v_x \cdot d\tau = \int_{\Delta T_0}^{\Delta T_{nucl}} \frac{A \cdot \Delta T^n}{\cos\theta + |\sin\theta|} \cdot \frac{d(\Delta T')}{G \cdot v_L} \tag{1}$$

$$\frac{A}{(n+1) \times G \times v_L \times (\cos\theta + |\sin\theta|)} \times (\Delta T_{nucl}^{n+1} - \Delta T_0^{n+1}) > d \tag{2}$$
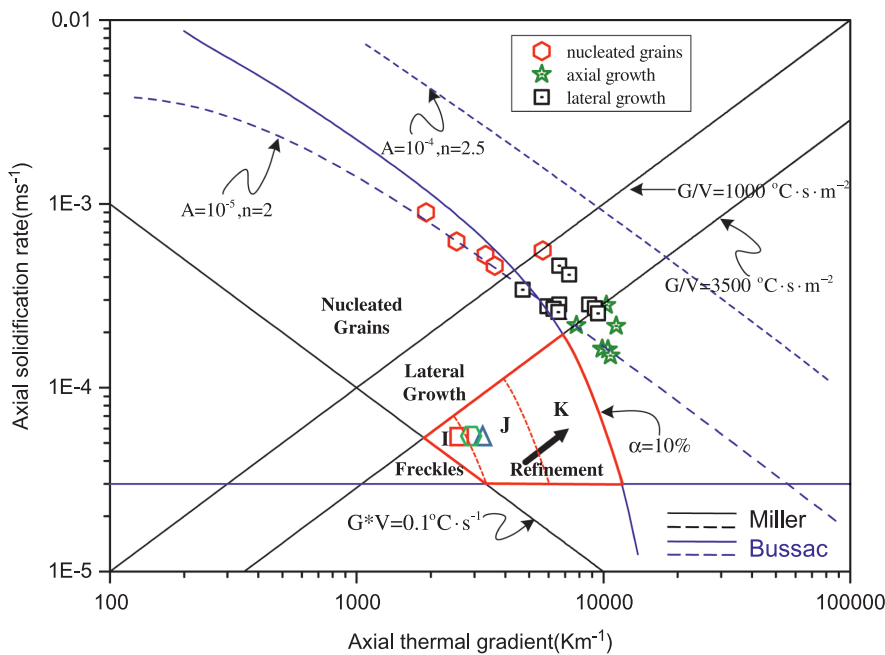
with, for converging dendrites

$$\Delta T_0 = \sqrt[n]{\frac{v_L}{A} \cdot \frac{1}{\cos\theta}} \tag{3}$$

and for diverging dendrites

$$\Delta T_0 = \sqrt[n]{\frac{v_L}{A} \cdot \frac{1}{(\cos\theta + |\sin\theta|)}} \tag{4}$$

where A and n are kinetics parameters depending on material properties and constitution, with respect to KGT model. The length $l(\Delta T_{nucl})$ is the integral over time of the velocity of the grain envelope in the direction of the x-axis, v_x, from the time when the grain starts to grow in the platform, t_0, to the time when the nucleation undercooling is reached, t_{nucl}. ΔT_0 and ΔT_{nucl} denote the undercooling of stationary growing grain interface envelop at time before approaching to the platform. θ is deviation angle between preference orientation of dendrite and withdrawing direction. G, v_L and d indicate temperature gradient, growing rate and length of platform, respectively. If temperature distribution involves lateral gradient α, the criteria changes to the form as shown in the appendix of reference [35]. The area of freckle formation and dendritic lateral growth located in process window (PW) is obtained from reference [36, 37].

However, as shown in Figures 7–9, the solidification process is not as simple as assumed, the early supercooling at platform end, the effect of tilt angle of mushy zone within airfoil and sophisticated geometrical structure are not taken into consideration in this model. Besides, the real process window with production acceptance criterion does not range as wide as presented, so it just has symbolic meaning in engineering application. The experimental and simulation results of this paper are mapped in modified process window, and the SX area are divided into three smaller parts (I, J and K), as shown in Figure 10. The temperature gradient (G) was calculated from the simulation results, and the solidification rate (V) was usually assumed to be approximately equal to the withdrawal rate. In previous researches, the areas in process window were usually divided by analytical method or fitted by the points of experimental results

	Cluster A △	Cluster B ⬠	Cluster C □
G(K/m)	3171.5	2941.2	2645.5
V(mm/min)	5	5	5

Figure 10: The modified process window in which SX area is divided into three more accurate parts — I, J and K.

and simulations. In this study, the points of different CMMCs was used to distinguish the suitable SX area for each CMMC upon control variants method. Cluster A is the worst construction manner, with three harmful effects taking place simultaneously and inducing the nucleation and growth of SG. Correspondingly, this lead to a great reduction of PW (I + J + K), indicated as area-I which doesn't contain the point of cluster A. But for cluster B, only shadow effect occurs according to the combination effect, so the mapped area shows no reduction and includes entire SX area in PW (I + J + K). As a CMMC better than cluster A, cluster C has shadow effect and channel effect, indicating a larger area in PW (I + J) which contains area-I.

Conclusion

In this study, both experiment and simulation were carried out to investigate the effect of CMMC on SG formation, as well as the mechanism of grain growth. The following conclusions can be drawn:

(1) By performing experiment, it is found that SG occurrence on platform is strongly influenced by the CMMC during directional solidification, despite the identical process parameters employed. Four samples in cluster A (0°) significantly exhibits more SGs than those in cluster B (45°) and C (90°).

(2) By means of numerical simulation, solidification sequences and paths were obtained to help analyse the process of grain growth and stray grain formation. Shadow effect, channel effect and dimension effect were proposed based on simulation results and in good agreement with the experimental phenomenon for different CMMCs.

(3) The combination effect reveals that the tendency for SG formation increases with the increase of the extent of the above three effects. This finding can be used to qualitatively predict SG occurrence in platform and improve the quality of SX component during directional solidification.

(4) Process window was modified, and the inside SX area was divided into three smaller parts to depict the influence of different factors on defects formation more accurately.

References

[1] L.H. Rettberg and T.M. Pollock, Acta mater., 73 (2014) 287–297.

[2] S. Gao, Z. Liu, C. Li, Y. Zhou and T. Jin, Acta Mater., 110 (2016) 268–275.

[3] X. Meng, J. Li, S. Zhu, H. Du, Z. Yuan, J. Wang, X. Sun and Z. Hu, Metall. Mater. Trans. A, 45A (2013) 1230–1237.

[4] M.C. Schneider, J.P. Gu, C. Beckermann, W.J. Boettinger and U.R. Kattner, Metall. Mater. Trans. A, 45A (2013) 1517–1531.

[5] D. Ma, Q. Wu and B.P. Andreas, Metall. Mater. Trans. B, 43B (2012) 344–357.

[6] L. Yuan and P.D. Lee, Acta Mater., 60 (2012) 4917–4926.

[7] R.C. Reed, The Superalloys: Fundamentals and Applications, Cambridge University Press, New York (2006).

[8] Z. Li, J. Xiong, Q. Xu, J. Li and B. Liu, J Mater Process Technol., 217 (2015) 1–12.

[9] X. Zhao, L. Liu, W. Zhang, M. Qu, J. Zhang and H. Fu, Rare Metal. Mat. Eng., 40 (2011) 9–13.

[10] X. Yang, D. Ness, P.D. Lee and N. D'Souza, Mater. Sci. Eng. A, 413–414 (2005) 571–577.

[11] X. Yang, P.D. Lee and N.D. Souza, JOM, 57 (2005) 40–44.

[12] J.W. Park, S.S. Babu, J.M. Vitek, E.A. Kenik and S.A. David, J. Appl. Phys., 94 (2003) 4203–4209.

[13] J.M. Vitek, Acta mater., 53 (2005) 53–67.

[14] T.D. Anderson, J.N. Dupont and T. Debroy, Metall. Mater. Trans. A, 41A (2010) 181–193.

[15] Y. Zhou, Scr. mater., 65 (2011) 281–284.

[16] X.L. Yang, H.B. Dong, W. Wang and P.D. Lee, Mater. Sci. Eng., A, 386 (2004) 129–139.

[17] X. Yan, N. Tang, X. Liu, G. Shui, Q. Xu and B. Liu, Acta Metall. sin, 51 (2015) 1288–1296.

[18] X. Meng, J. Li, T. Jin, X. Sun, C. Sun and Z. Hu, J. Mater. Sci. Technol., 27 (2011) 118–126.

[19] N. Wang, L. Liu, S. Gao, X. Zhao, T. Huang, J. Zhang and H. Fu, J. Alloys Compd., 586 (2014) 220–229.

[20] M.M. Ter Vehn, D. Dedecke, U. Paul and P.R. Sahm, Superalloy TMS, (1996) 471–479.

[21] D. Ma, S. Hollad and A.B.- Polaczek, Metall. Mater. Trans. B, 40B (2009) 738–748.

[22] S. Simmonds, Formation and Avoidance of Surface Defects During Casting and Heat-Treatment of Single-Crystal Nickel-Based Superalloys, Ph. D Thesis (2013).

[23] N. D'Souza, M. Newell, K. Devendra, P.A. Jennings, M.G. Ardakani and B.A. Shollock, Mater. Sci. Eng. A, 413–414 (2005) 567–570.

[24] J. Zhao, J. Li, S. Liu, H. Yuan and M. Han, J. Aero. Mater., 27 (2007) 6–10.

[25] Z. Shi, J. Li, S. Liu and J. Zhao, Rare Metal. Mat. Eng., 41 (2012) 962–966.

[26] Z. Li, Q. Xu and B. Liu, Mater. Today Proc., 2 (2015) 440–452.

[27] J. Li, J. Xiong and D. Tang, Advanced High Temperature Structural Materials and Technology, National Defense Industry Press, Beijing (2012).

[28] Editorial Committee of Engineering Materials Handbook, Standards Press of China, Beijing (2001).

[29] D. Ma, Acta Metall. Sin., 51 (2015) 1179–1190.

[30] T.M. Pollock, Metall. Mater. Trans. A, 35A (2004) 3221–3231.

[31] N. Tang, Y. Wang, Q. Xu, X. Zhao and B. Liu, Acta Metall. Sin., 51 (2015) 499–512.

[32] D. Ma, Acta Metall. Sin., 52 (2016) 426–436.

[33] X. Meng, J. Li, Z. Chen, Y. Wang, S. Zhu, X. Bai, F. Wang, J. Zhang, T. Jin, X. Sun and Z. Hu, Metall. Mater. Trans. A, 44A (2012) 1955–1965.

[34] W. Kurz, B. Giovanola and R. Trivedi, J. Cryst. Growth, 91 (1988) 123–125.

[35] A. de Bussac and C.A. Gandin, Mater. Sci. Eng. A, 237 (1997) 35–42.

[36] T.M. Pollock and W.H. Murphy, Metall. Mater. Trans. A, 27A (1996) 1081–1094.

[37] J.D. Miller and T.M. Pollock, Acta Mater., 78 (2014) 23–36.